Published in : Thin-Walled Structures (2021), vol. 159, 107287
DOI: 10.1016/j.tws.2020.107287
Status : Postprint (Author's version)

EXPERIMENTAL AND NUMERICAL INVESTIGATIONS ON LARGE ANGLE HIGH STRENGTH STEEL COLUMNS

Marios-Zois Bezas [a,b,*], Jean-François Demonceau [a], Ioannis Vayas [b], Jean-Pierre Jaspart [a]

[a] *Steel and Composite Construction, UEE Research Unit, Liege University, Belgium*

[b] *School of Civil Engineering, Institute of Steel Structures, National Technical University of Athens, Athens, Greece*

Keywords :
Stability, Angle cross-section, High-strength steel, Experimental investigations, Numerical simulations, Eurocode 3

Abstract
The stability of columns made of large angle profiles in high strength steel and subjected to centric and eccentric compression loads is investigated through experimental tests, numerical simulations and normative approaches. The aim is to widen the knowledge on such columns and so to complement previous experimental studies that focusing on smaller angle profiles and lower steel grades. The experimental campaign consists of twelve tests. Accompanying numerical studies have been carried out, considering relevant geometrical imperfections as well as geometrical and material non-linearities. Finally, an assessment of the design member resistance according to Eurocodes has been performed. It is further discussed.

Published in : Thin-Walled Structures (2021), vol. 159, 107287
DOI: 10.1016/j.tws.2020.107287
Status : Postprint (Author's version)

1. Introduction

Angles profiles have been used since the very beginning of steel construction due to their easy transportation and on-site erection. They are extensively used in lattice towers and masts for telecommunication purposes or electric power transmission, as well as in a wide range of civil engineering applications such as buildings and bridges. They are also used to strengthen existing structures. Recent developments in transmission towers, like the installation of new 380-kV lines or high- voltage direct current (HVDC) lines, lead to the need for a wider application of large angle sections made of high strength steel. In Europe, lattice towers are designed to different standards. Generally, steel lattice towers are designed to Eurocodes and in particular to EN 1993-3-1 [1], in combination with EN 1993-1-1 [2] providing general rules and EN 1993-1-8 [3] providing rules for connections. But in the specific field of overhead electrical lines, lattice towers are designed to CENELEC standard EN 50341-1 [4] which provides rules sometimes diverging from those proposed in the Eurocodes. However, in all preceding codes, rules concern angles subjected to pure compression and bending effects due to eccentric connection in one angle, being considered through a modification of the buckling length. Eurocode 3 proposes a so-called "general method for lateral and lateral torsional buckling of structural components" which could possibly be applied to angle columns under compression and bending. In contrast, American codes [5] have issued design specifications for single angle members subjected to general loading conditions including compression and bending.

Compression tests on large angle sections ranging from L125 × 125 × 8 to L200 × 200 × 14 in high strength steel (HSS) S420 were conducted in Tsinghua University in Beijing [6]. The tests were carried out on axially loaded pin-ended columns in order to define global-local buckling interactions since cross-sections were in many cases class-4 ones. Tests on L70 × 70 × 7 profiles were performed at NTUA in Athens [7], where the effects of eccentric loading were studied. Compression tests on L80 × 80 × 8 and L120 × 120 × 12 profiles were carried out at TU Graz [8] in which the boundary conditions were varying from clamped supports to supports allowing in-plane or in- and out-of-plane rotation. A tests series on L50 × 50 × 5 profiles were carried out at the Technical University of Braunschweig [9] with various specimen lengths and end support conditions, while the load was introduced eccentrically through one bolt M12 in one leg. A series of compression tests was performed on equal angle profiles loaded through two bolts in one leg at the University of Windsor, Canada [10]. The cross-sections were L64 × 64 × 4.8, L64 × 64 × 6.4 and L76 × 76 × 6.4 with steel material S300. The bolts were fastened snug-tight or preloaded. Further tests were performed at the same University, where the angles were loaded through one bolt [11]. The cross-sections were equal angle profiles L51 × 51 in three thicknesses, 4.8, 6.4 and 7.9, L64 × 64 in two thicknesses, 6.4, 7.9 and L76 × 76 × 6.4. The material was also steel S300, as in the previous tests [10]. All nominal dimensions of the above-mentioned cross-sections of tested columns were in mm.

In order to study the stability behaviour of steel columns from HSS (S460M) angle cross-sections subjected to compression and bending, twelve (12) buckling tests on such columns have been performed. The experiments have been limited to high strength steel only, given the fact that a number of compression tests on angles with lower steel grades were already available. The test campaign has been realized at the

Published in : Thin-Walled Structures (2021), vol. 159, 107287
DOI: 10.1016/j.tws.2020.107287
Status : Postprint (Author's version)

"Laboratoire de Mécanique des Matériaux et Structures" at Liège University. The selection of the specimens, the details about the experimental campaign such as measurements before and during the tests, as well as the test results, are presented and discussed in this article. The tests have been accompanied by numerical simulations performed with the full non-linear finite element software FINELG, considering relevant imperfections as well as geometrical and material non-linearities. The numerical results have been compared and validated with the experimental ones. Finally, a comparison between the experimental ultimate member resistances and the Eurocode predictions for centrally and eccentrically loaded columns is presented and discussed. The experimental campaign and the numerical simulations are part of the European project ANGELHY, an RFCS-supported research project dealing with lattice telecommunication and transmission towers and lattice girders from angle sections.

2. Details of tested specimens

For the experimental program, two profiles from large angle cross-sections made of S460M steel grade have been selected. For each profile, six (6) column tests have been performed with three (3) different lengths per profile and two (2) positions of load application for each length. The selected points are (see **Fig. 1**) the centre of gravity (G), which corresponds to pure compression in the angle cross-section and the intersection point of minor principal axis v-v with the middle line of the leg thickness (P_2), which represents the position of the connecting bolt for angles in structures.

Table 1 summarizes all the details about the specimens. The name of each specimen consists of two numbers Sp## (e.g. Sp12):

- the first number indicates the profile: 1 for L150 × 150 × 18 and 2 for 200 × 200 × 16;
- the second one is the serial number of the specimen (1 to 6 per profile).

For all tests, constant dimensions have been selected for the end plates welded at the extremities of the angle members, in order to simplify the placement procedure of the specimen in the test rig. Therefore, the position of the applied load is always the same for the machine and the eccentricity is introduced by moving the profile on the end plates. The steel grade of all end plates is S355 and not S460M as for the profiles. The welds have been designed according to EN 1993-1-8 [12]. For all specimens, the minimum required weld thickness is 6 mm, except for specimens Sp11 and Sp21 which require a minimum thickness of 8 mm. **Fig. 2** shows the details of such end plates on which the specimens have been welded.

Published in : Thin-Walled Structures (2021), vol. 159, 107287
DOI: 10.1016/j.tws.2020.107287
Status : Postprint (Author's version)

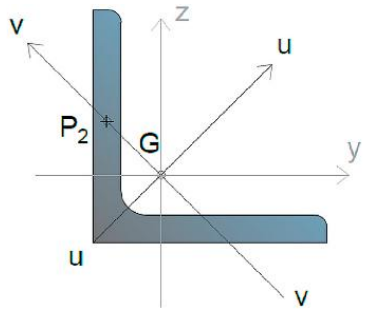

G centre of gravity
P_2 the middle of the wall
u-u major principal axis (weak axis displacement)
v-v minor principal axis (strong axis displacement)
y,z geometrical axes

Fig. 1. Position of applicable load and definition of the axes.

Table 1
Details about the specimens.

ID of Specimen	Profile	Steel grade	Angle member length L [mm]	Eccentricity [mm]
Sp11	L 150 × 150 × 18	S460M	2500	0,00
Sp12	L 150 × 150 × 18	S460M	2500	e_v = 48,74
Sp13	L 150 × 150 × 18	S460M	3000	0,00
Sp14	L 150 × 150 × 18	S460M	3000	e_v = 48,74
Sp15	L 150 × 150 × 18	S460M	3500	0,00
Sp16	L 150 × 150 × 18	S460M	3500	e_v = 48,74
Sp21	L 200 × 200 × 16	S460M	3000	0,00
Sp22	L 200 × 200 × 16	S460M	3000	e_v = 66,64
Sp23	L 200 × 200 × 16	S460M	3500	0,00
Sp24	L 200 × 200 × 16	S460M	3500	e_v = 66,64
Sp25	L 200 × 200 × 16	S460M	4000	0,00
Sp26	L 200 × 200 × 16	S460M	4000	e_v = 66,64

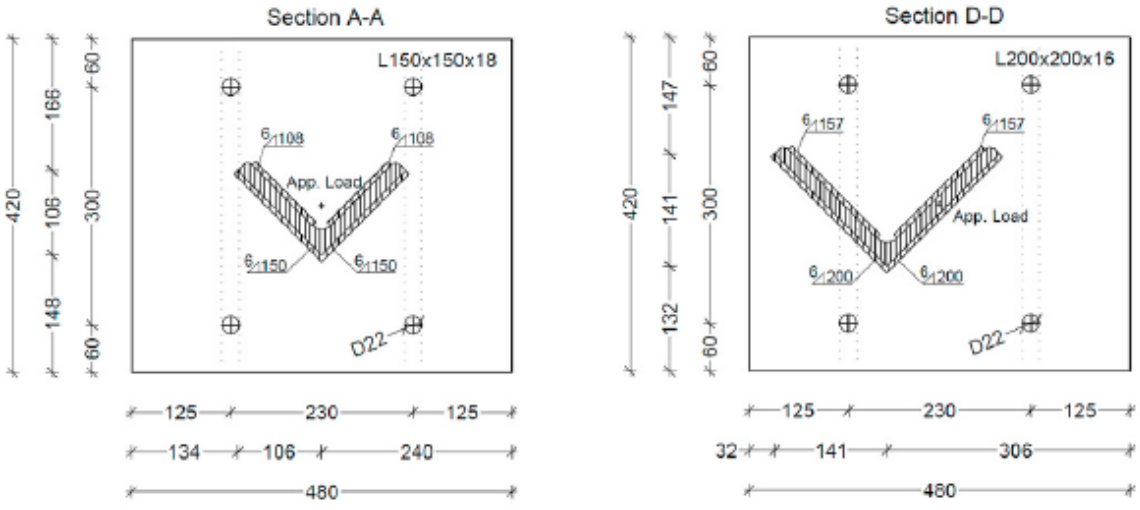

Fig. 2. Detail of end plates in case of centrally (left) and eccentrally (right) loaded specimens.

Published in : Thin-Walled Structures (2021), vol. 159, 107287
DOI: 10.1016/j.tws.2020.107287
Status : Postprint (Author's version)

3. Measurements before and during a test

3.1. ACTUAL DIMENSIONS OF THE CROSS-SECTIONS

The actual geometrical dimensions of each angle section – the width (b_i) and the thickness (t_i) of each leg – have been measured at 3 points along the member: at 1/4, 1/2 and 3/4 of the angle member length (L). The mean values of the measurements are reported in **Table 2**. The length and the load eccentricity of each specimen has been also measured and reported in **Table 2**.

Table 2
Measurements of the actual geometry and dimensions of the cross-sections.

ID of specimen	Length [mm]	Eccentricity [mm]	b_A [mm]	b_B [mm]	t_A [mm]	t_B [mm]
Sp11	2500	0,00	149,97	150,09	18,16	18,14
Sp12	2500	e_v = 48,71	150,07	150,12	18,18	18,04
Sp13	3000	0,00	150,11	149,92	18,04	18,16
Sp14	3000	e_v = 48,72	150,09	150,10	18,04	18,17
Sp15	3500	0,00	150,07	150,11	18,17	18,07
Sp16	3500	e_v = 48,70	150,11	149,95	18,16	18,19
Sp21	3000	0,00	200,31	200,41	16,32	16,34
Sp22	3000	e_v = 66,60	200,36	200,39	16,39	16,29
Sp23	3500	0,00	200,25	199,92	16,32	16,28
Sp24	3500	e_v = 66,65	200,05	200,01	16,42	16,10
Sp25	4000	0,00	199,96	200,27	16,33	16,35
Sp26	4000	e_v = 66,63	200,06	200,39	16,32	16,31

$b_i = 1/3(b_{iL1}/4+b_{iL1}/2+b_{iL3/4})$ $(i = A,B)$; $t_i = 1/3(t_{iL1}/4+t_{iL1}/2+t_{iL3}/4)$ $(i = A,B)$.

3.2. MEASUREMENT OF INITIAL GEOMETRICAL IMPERFECTIONS ALONG THE MEMBER LENGTH

Two displacement measurements (M1 & M2) on each external face (Face A & Face B) and along the column length have been performed so as to evaluate the initial imperfections of the specimens. **Fig. 3** shows the details of the set-up. Due to the end plates and the measurement system itself, it was not possible to take measurements quite close to the ends of the specimens. As a result, all the measurements start 140 mm after the top end plate and finish 140 mm before the bottom one. A measurement has been taken every 50 mm along the column. It has been quite reasonably assumed that the columns are straight close to the end plates (140 mm).

As the chariot supporting the displacement transducers was moving onto a horizontal guiding bar, a small rotation of the metric system was occurring; this one has been measured with an inclinometer, so allowing correcting the measurements accordingly. In addition, the column was not perfectly parallel to the set-up. For those reasons, the first correction to achieve concerned the non-parallelism and the rotation of the metric system; it is based always on the position of a reference cable. Then, a second correction has been done in order to have zero imperfection at the extremities of the column. Finally, a horizontal movement of the curve has been achieved so that the first measurement is well

Published in : Thin-Walled Structures (2021), vol. 159, 107287
DOI: 10.1016/j.tws.2020.107287
Status : Postprint (Author's version)

reported at 140 mm of the end plate. This procedure has been followed for face A and face B. All the results from the measured geometrical imperfections can be found in Ref. [13]. An example of the initial measurements and the evaluated geometrical imperfections of Specimen 15 are presented in **Fig. 4** and **Fig. 5** respectively.

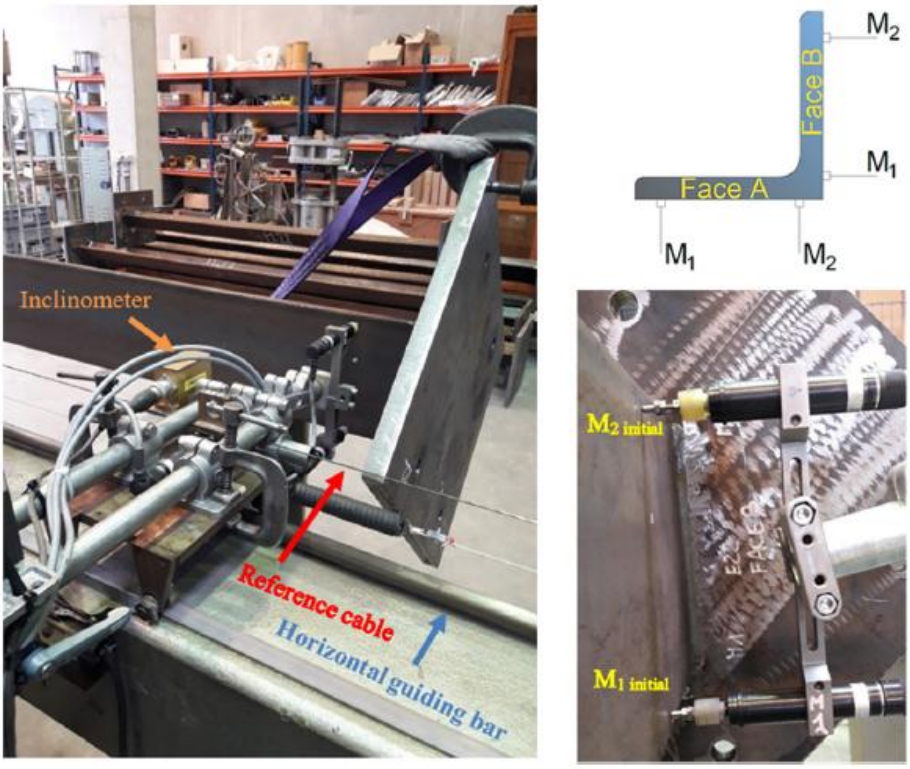

Fig. 3. Measurement system for geometrical imperfections (left), detail and position of the displacement transducers (right).

An accurate comparison between the actual measured imperfections of the specimens and those assumed in the Eurocode is quite difficult to do. The European norm EN 1090-2 [14] prescribes that the deviation from straightness should be $\Delta \leq L[mm]/750$ while in prEN 1993-1-14 [15] it is stated that 80% of the geometric fabrication tolerances given in Ref. [14] should be applied. This leads to an initial bow imperfection of magnitude approximately equal to L[mm]/1000 and usually a deformation shape similar to the first member instability mode is assumed, however in reality the shape is more complex. For this reason, only a rough comparison can be done at this level (see **Table 3**) through the evaluation of an experimental estimated value $|Max|_{imperf}$ obtained by taking into account the maximum value [M_{1CA}, M_{1CB}, M_{2CA}, M_{2CB}] and by assuming that it is the same in both faces:

$$|Max|_{imperf} = \max\{M_{1CA},\ M_{2CA},\ M_{1CB},\ M_{2CB}\}\cdot\sqrt{2} \qquad (1)$$

where:

M_{1CA} is the M_1 maximum final corrected measurement on face A for specimen i;
M_{2CA} is the M_2 maximum final corrected measurement on face A for specimen i;
M_{1CB} is the M_1 maximum final corrected measurement on face B for specimen i;

Published in : Thin-Walled Structures (2021), vol. 159, 107287
DOI: 10.1016/j.tws.2020.107287
Status : Postprint (Author's version)

M_{2CB} is the M_2 maximum final corrected measurement on face B for specimen i.

Then, it can be concluded that measured imperfections are smaller for all specimens than the geometrical tolerances prescribed in European regulations.

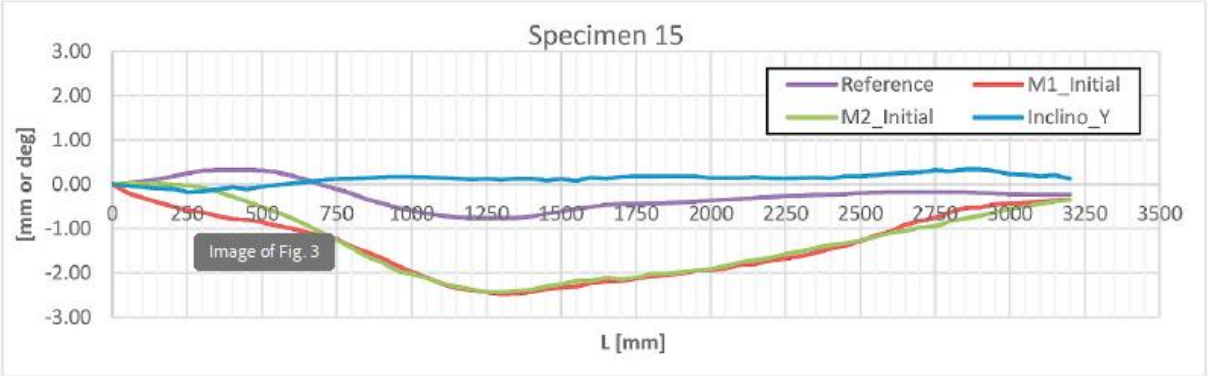

Fig. 4. Initial measurements of geometrical imperfections for Sp15-face B.

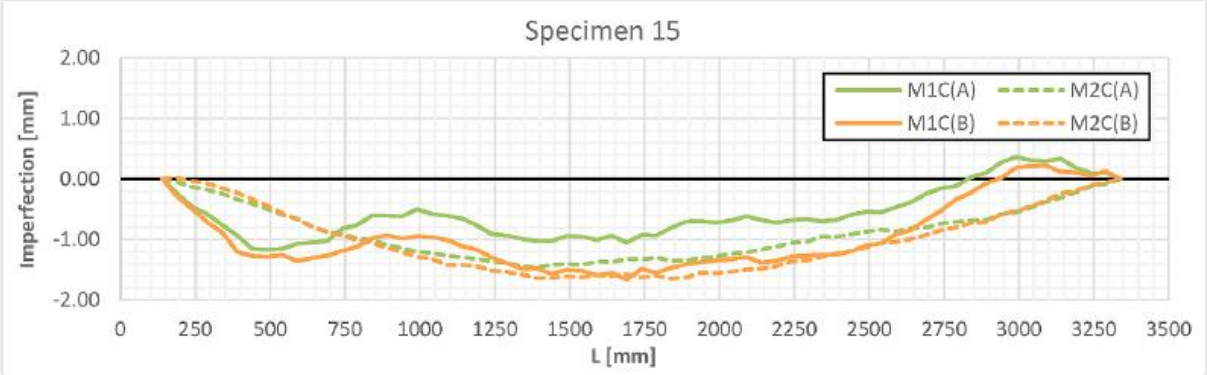

Fig. 5. Initial geometrical imperfections of both faces along specimen 15.

Table 3
Maximum values of the actual initial imperfections of the specimens compared with those prescribed by the European regulations [14,15].

ID of specimen	L/1000 [mm]	$\|Max\|_{imperf}$ [mm]
Sp11	2,5	0,4
Sp12	2,5	1,2
Sp13	3,0	1,3
Sp14	3,0	0,8
Sp15	3,5	2,4
Sp16	3,5	3,0
Sp21	3,0	1,6
Sp22	3,0	2,7
Sp23	3,5	1,7
Sp24	3,5	2,8
Sp25	4,0	1,5
Sp26	4,0	1,8

Published in : Thin-Walled Structures (2021), vol. 159, 107287
DOI: 10.1016/j.tws.2020.107287
Status : Postprint (Author's version)

3.3. COUPON TESTS FOR THE MATERIAL PROPERTIES

Coupon tests have been performed in accordance with ISO 6892- 1:2016 [16]. The samples for the tensile tests have been extracted from one of the extremities of the angle member (see **Fig. 6**) after the buckling tests, based on ISO 377:1997 [17].

Fig. 7 shows the strain-stress curves obtained from few tensile tests and **Table 4** provides the characteristic values for all. The yield stress f_y (engineering stress) is determined by the value of the yield plateau in the curves and defers from the upper value yield stress ReH. It may be also observed that while the actual ultimate stress was for all specimens above the nominal values, this was not true for the yield stress.

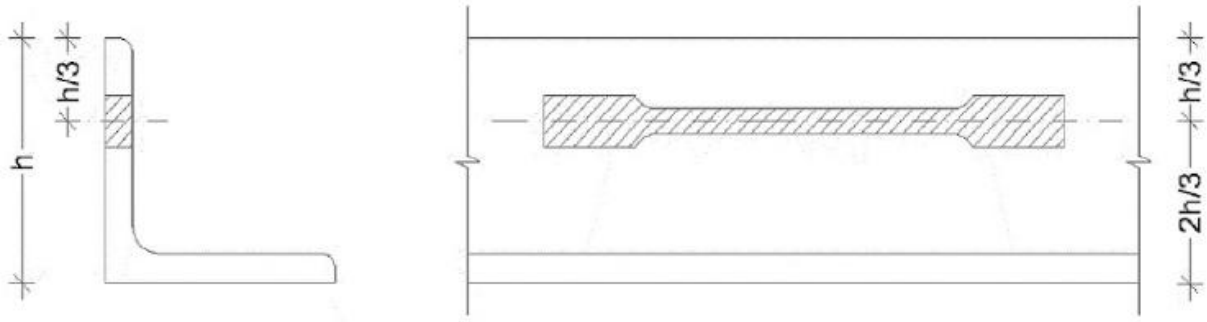

Fig. 6. Location of tensile samples for coupon tests based on Ref. [17].

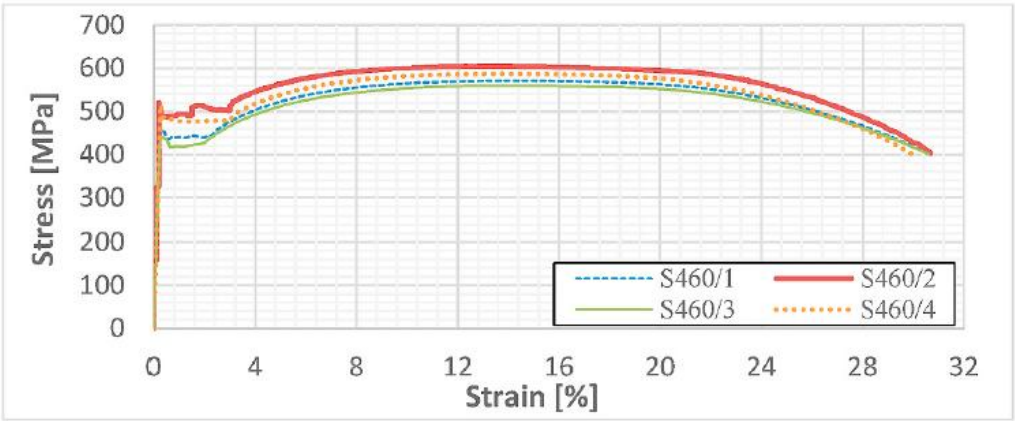

Fig. 7. Stain-stress curves from the coupon tests.

Table 4
Coupon test's results.

ID of material	E [MPa]	Measured yield stress f_y [MPa]	Measured ultimate stress f_{ult} [MPa]	Measured strain at failure [%]	Nominal yield stress $f_{y,nom}$ [MPa]	$f_y/f_{y,nom}$ [−]	Characterized specimens
S 460/1	203155	425,8	572,50	14,3	460,0	0,93	Sp12, Sp13, Sp14, Sp15, Sp16
S 460/2	208947	487,6	604,64	13,7	460,0	1,06	Sp21, Sp22, Sp23, Sp25, Sp26
S 460/3	197317	417,2	560,87	14,3	460,0	0,91	Sp11
S 460/4	203797	472,6	587,21	13,8	460,0	1,03	Sp24

Published in : Thin-Walled Structures (2021), vol. 159, 107287
DOI: 10.1016/j.tws.2020.107287
Status : Postprint (Author's version)

3.4. MEASUREMENTS DURING THE TEST

The tests have been carried out in an Amsler 500 testing machine, with a compression capacity of 5000 kN. The specimens are pin-ended in the testing rig, since the rotations about the minor and major axes can develop freely, but no twist or warping is able to occur at the extremities. During the tests, the following displacements illustrated in **Fig. 8** were measured:

- the vertical displacement C_1 (using two transducers, one at the front and one at the back side of the specimen);
- four horizontal displacements C_2, C_3, C_4 and C_5 at the mid cross- section (1st position);
- four horizontal displacements C_6, C_7, C_8 and C_9 at the lower cross- section (2nd position).

All the displacement transducers have been placed 30 mm from the edges/corner of all cross-sections and profiles. The set-up allowing the record of those displacements is illustrated in **Fig. 9**. In addition, four strain gauges (I_1 to I_4) have been placed at the mid-height cross-section of each column, in order to check local yielding. The strain gauges have been positioned as close as possible to the edges of the cross-section, taken into account the curvature of the latter.

3.5. MATHEMATICAL INTERPRETATION OF THE MEASUREMENTS

The displacements of the corner of the angle (O point) as well as the twist of the cross-section, that are reported in the graphs of section 4.1, have been evaluated using the following formulae (for the definition of the axes and symbols, see **Fig. 10** left):

$$y_O = C_3 + 30 \cdot \frac{C_3 - C_2}{d} [mm] \quad (2)$$

$$z_O = C_4 - 30 \cdot \frac{C_5 - C_4}{d} [mm] \quad (3)$$

$$\theta = \frac{1}{2}\left(atan\left(\frac{C_3 - C_2}{d}\right) + atan\left(\frac{C_5 - C_4}{d}\right)\right) \cdot 1000 [mrad] \quad (4)$$

where d = 90 or 140 [mm] for L150 × 150 × 18 or L200 × 200 × 16. The formulae are given for the middle cross-section, but they may also be used for the lower one, by replacing C_2, C_3, C_4 and C_5 by C_6, C_7, C_8 and C_9 respectively.

To transform the displacements from the geometrical axes to the principal ones (see **Fig. 10** right), the following equations have been used, for an angle equal to 45°.

$$u_i = y_i cos\theta + z_i sin\theta = (y_i + z_i) \cdot \frac{\sqrt{2}}{2} \quad (5)$$

$$v_i = z_i cos\theta - y_i sin\theta = (z_i - y_i) \cdot \frac{\sqrt{2}}{2} \quad (6)$$

Published in : Thin-Walled Structures (2021), vol. 159, 107287
DOI: 10.1016/j.tws.2020.107287
Status : Postprint (Author's version)

The axial deformation of the specimen has been evaluated as the mean value of both vertical transducers.

4. Results, comparisons and discussions

The results of the experimental tests are presented below through graphs and tables. Numerical simulations of the tests have been performed with FINELG software, taking into account the actual dimensions, length, imperfection and material properties. A comparison between the ultimate resistances obtained experimentally and through EN 1993-1-1 predictions has also been achieved for centrally and eccentrically loaded columns.

4.1. RESULTS OF THE EXPERIMENTAL TESTS

Fig. 11 and **Fig. 12** show the load-axial displacement (shortening) curves for the profiles L150 × 150 × 18 and L200 × 200 × 16 respectively. All the measurements (initial geometrical imperfections, rotations, strains and deflections) for each specimen are available in Ref. [13].

Both figures indicate that the results obtained by experimentation are in line with the physical expectations (for instance, the influence of the member length and of the eccentricity on the member stiffness and resistance properties). This seems a priori to validate the initial selection of the different parameters in the test campaign.

Amongst the specimens without nominal loading eccentricity, three (Sp11, Sp15, Sp25) showed nearly zero and three (Sp13, Sp21, Sp23) very small deflections transverse to the weak axis (see **Fig. 13**). This may indicate that only three specimens were almost loaded without any eccentricity, while the other three had probably some unintentional eccentricity resulting from installation tolerances as explained later. Nevertheless, for all the tests, the deflections along weak axis increased significantly with the load until failure was reached by weak axis buckling; towards the heel of the cross section for Specimens Sp13, Sp15, Sp25 and in the opposite direction for Sp11, Sp21 and Sp23. Concluding, specimens Sp11, Sp13 and Sp15 failed in a pure flexural buckling mode (see **Fig. 15**(a)), while in specimens Sp21, Sp23 and Sp25 twist rotations were recorded (see **Fig. 14**), and in addition to weak axis deflections indicating a flexural torsional buckling mode.

The eccentrically loaded specimens were initially subjected to compression and strong axis bending. At low load levels, the deflections transverse to the strong axis were high and very small in the other principal direction (see **Fig. 16** and green cross-sections in **Fig. 17**). However, this was opposite to the tendency of the angles to fail by weak axis buckling. At higher load levels, deflections transverse to the weak axis grew quickly and prevailed at failure (in **Fig. 17**, the red cross-section corresponds to the ultimate load and the blue cross-section is after buckling). In the specimens Sp22, Sp24 and Sp26 these deflections were accompanied by significant twist rotations indicating clearly failure with a flexural-torsional buckling mode (see **Fig. 15**(b)). On the contrary, twist rotations were small for specimens Sp12, Sp14 and Sp16 indicating a mixed mode between flexural and flexural torsional buckling (see **Fig. 15**(c)). The most stressed mid-height cross section was subjected to compression and bi-axial bending.

Published in : Thin-Walled Structures (2021), vol. 159, 107287
DOI: 10.1016/j.tws.2020.107287
Status : Postprint (Author's version)

In fact, strong axis bending was primarily due to the eccentric loading and weak axis bending due to second order effects.

The absence of visible local buckling in all specimens should be also mentioned.

Finally, **Table 5** presents for each specimen the measured failure load (N_{exp}) as well as the deflections about minor (v_O) and major (u_O) principal axes and the twist at the mid-height cross-section, all at the failure load. The sign of the deflections and the twist is in accordance with **Fig. 10**.

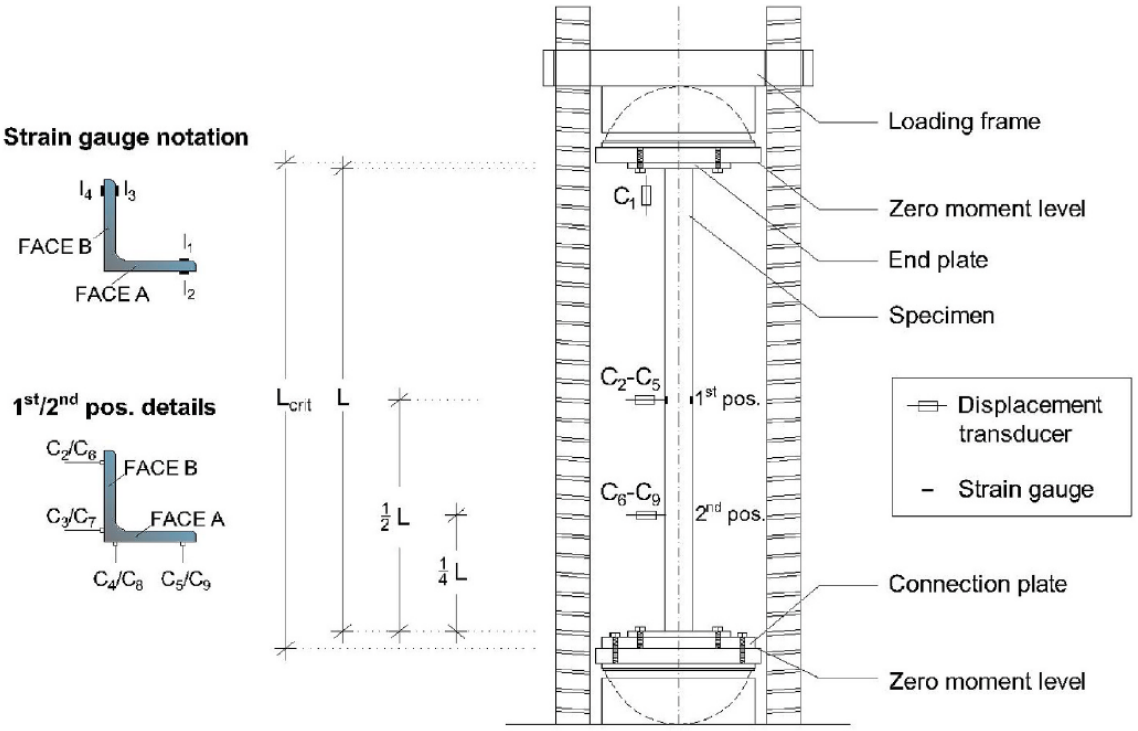

Fig. 8. Sketch of Amsler 500 test machine and measurements during a test.

Published in : Thin-Walled Structures (2021), vol. 159, 107287
DOI: 10.1016/j.tws.2020.107287
Status : Postprint (Author's version)

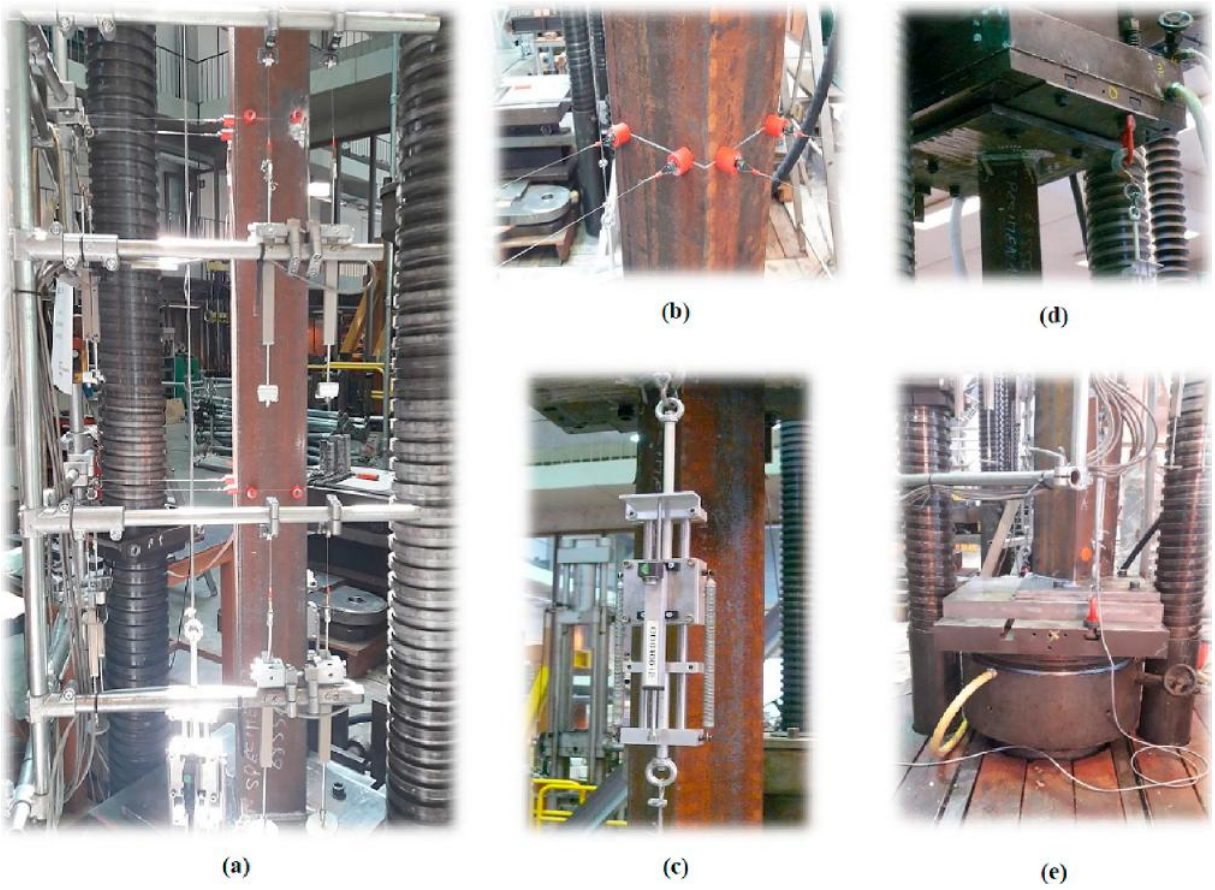

Fig. 9. (a) General view of test rig with the measurement devices, (b) connection points of displacement transducers on the cross-section, (c) vertical displacement transducer, (d) detail of the top bearing plate and (e) detail of the bottom bearing plate.

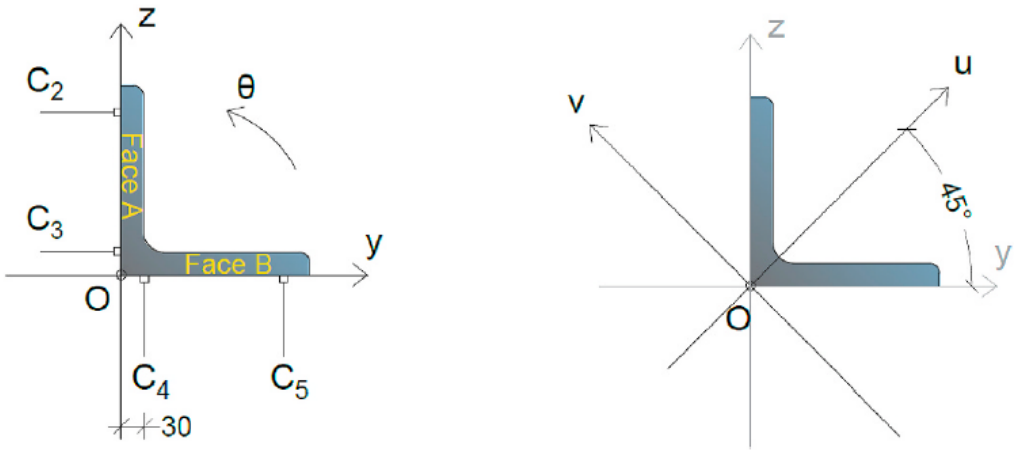

Fig. 10. Definition of axis and symbols for the mathematical interpretation.

Published in : Thin-Walled Structures (2021), vol. 159, 107287
DOI: 10.1016/j.tws.2020.107287
Status : Postprint (Author's version)

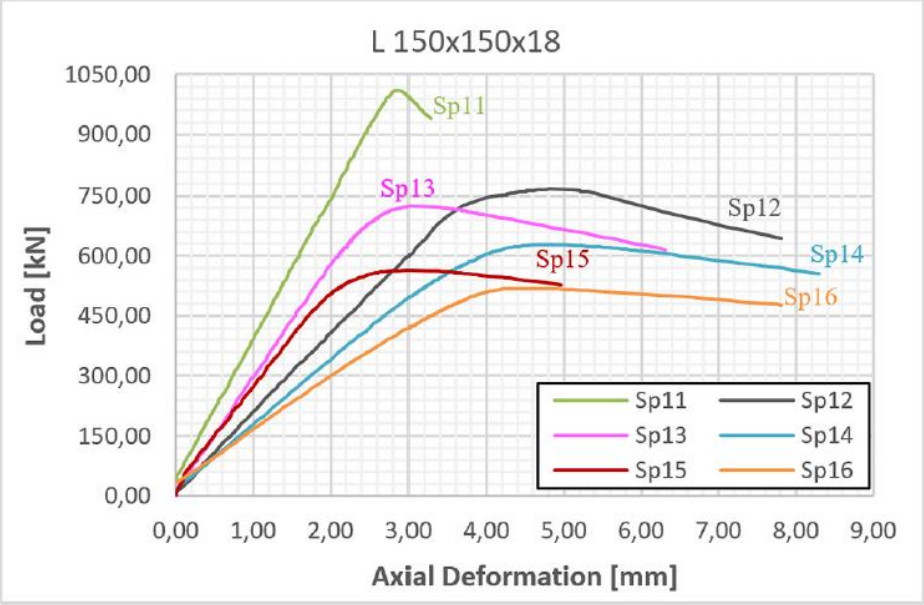

Fig. 11. Load vs axial deformation of tested profiles L 150 × 150 × 18.

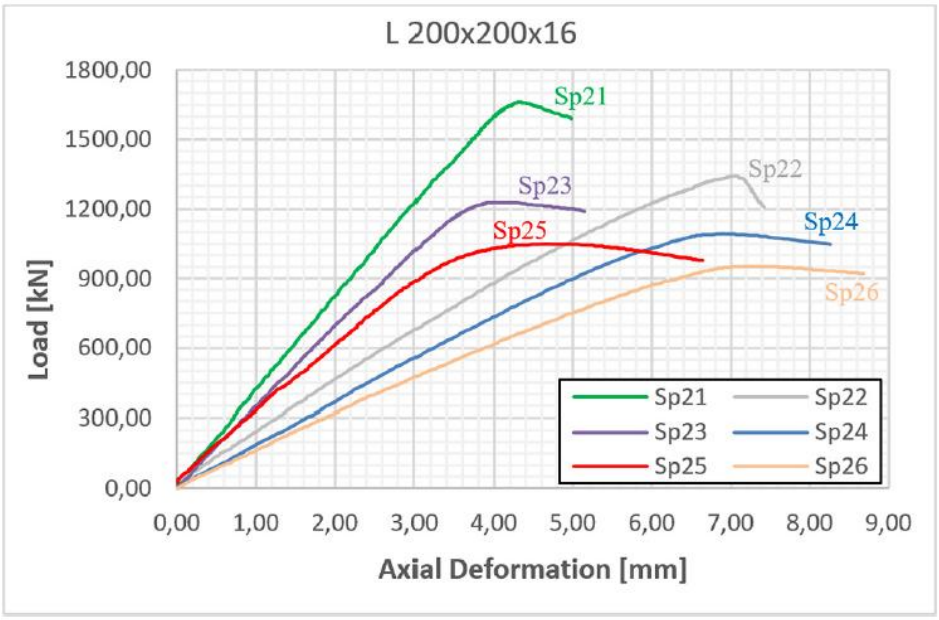

Fig. 12. Load vs axial deformation of tested profiles L 200 × 200 × 16.

4.2. COMPARISON WITH FEM ANALYSES

Subsequently, numerical simulations considering relevant imperfections as well as geometrical and material non-linearities were performed and compared with the results of the experimental tests. The numerical analyses were performed with FINELG non-linear finite element software [18] using beam elements. The choice of beam elements is acceptable and justified from the fact that no local buckling took place during the tests. The FINELG software was selected due to its wide and successful use in the past for such a type of analyses [19]. Only the column has been modelled while the end plates at the extremities have been considered indirectly. Each column has been meshed in twenty beam finite

Published in : Thin-Walled Structures (2021), vol. 159, 107287
DOI: 10.1016/j.tws.2020.107287
Status : Postprint (Author's version)

elements along the member length. This is an optimal mesh as the difference of member's response (ultimate load and deflections) is less than 1% ether the member is meshed in fifteen elements or thirty. The length (L) of each column has been increased by 107 mm, what corresponds to the thickness of the end plates of the specimens as well as the connection plate, so as to simulate the actual buckling length (L_{crit}) of the column (length between the zero moment levels in **Fig. 8**). The columns were assumed as pin-end members with free rotations at their extremities, except the rotation that leads to torsion along the length axis, which was blocked. All the other DOF at the extremities were blocked, except u_x of the node of the applied load. Therefore, the experimental boundary conditions were rather well represented by the model.

The FINELG finite element analyses adopting the GMNIA method were performed considering:

- an initial member imperfection (shape and magnitude in accordance with the measured ones);
- residual stresses resulting from the hot-rolling procedure. The selected pattern (**Fig. 18**) is chosen from previous studies [20,21] in which appropriate measurements had been realized; It has to be taken into account that the residual stresses in hot rolled steel sections are independent of the steel grade and therefore a magnitude of $0{,}15 \cdot f_y$, that is approximately equal to 70 MPa for steel grade S460, is used. The selected pattern is applied automatically by the software to each beam element along the member length.
- a material law in accordance with the measured one (see **Table 4**).

A tolerance on the position of the applied load from up to 2,0 mm has been adopted for the numerical simulations in order to calibrate the results. It has been found that even a small eccentricity could affect the ultimate resistance and the stiffness of the member in comparison to the perfectly "no loading eccentricity" case. **Fig. 19** shows that an eccentricity equal to 1,5 mm (for the angle section L200 × 200 × 16) is able to change the ultimate resistance by approximately 6%. The influence of this small eccentricity of the applied load on the stiffness and the ultimate resistance has been also observed in Ref. [22]. The eccentricity has been applied in u direction as it has been found through numerical simulations that the influence on the response of an eccentricity in the v direction is negligible (see **Fig. 1** for the definition of the axes). This tolerance could be explained by the two following reasons:

- the nominal position of the load has been designed to coincide with the centre of the end plates and accordingly with the centre of gravity of the cross section. In reality, due to small differences of the cross- section geometry, the real centre of gravity does not coincide exactly with the loading point;
- the positioning of the specimen in the testing rig may also induce a small and unexpected eccentricity.

Published in : Thin-Walled Structures (2021), vol. 159, 107287
DOI: 10.1016/j.tws.2020.107287
Status : Postprint (Author's version)

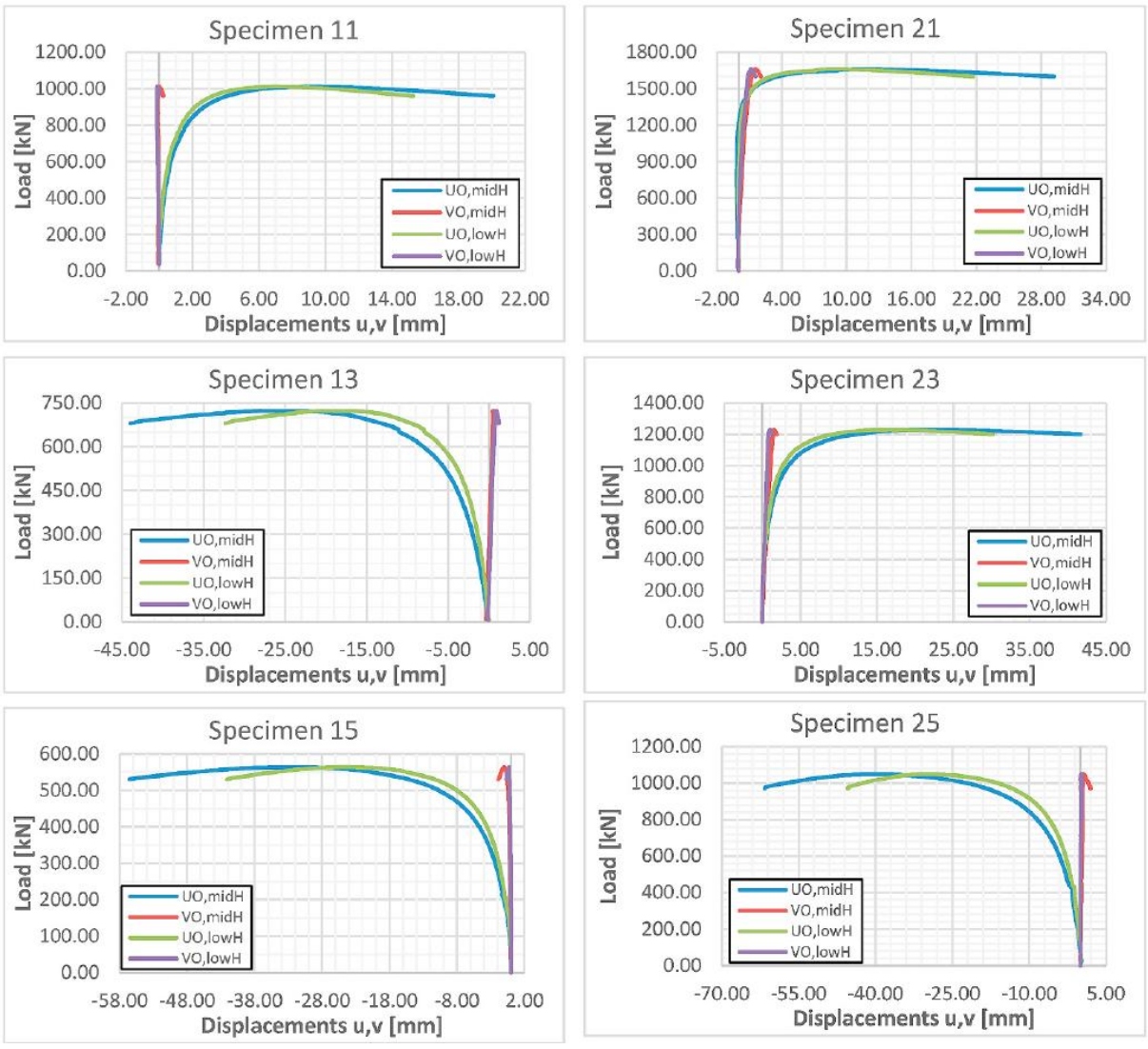

*$U/V_{O,midH}$ is the displacement of the corner point O of the mid – height cross-section along u/v principal axis

*$U/V_{O,lowH}$ is the displacement of the corner point O of the low – height cross-section along u/v principal axis

Fig. 13. Load-deflection curves for centrally loaded specimens.

Published in : Thin-Walled Structures (2021), vol. 159, 107287
DOI: 10.1016/j.tws.2020.107287
Status : Postprint (Author's version)

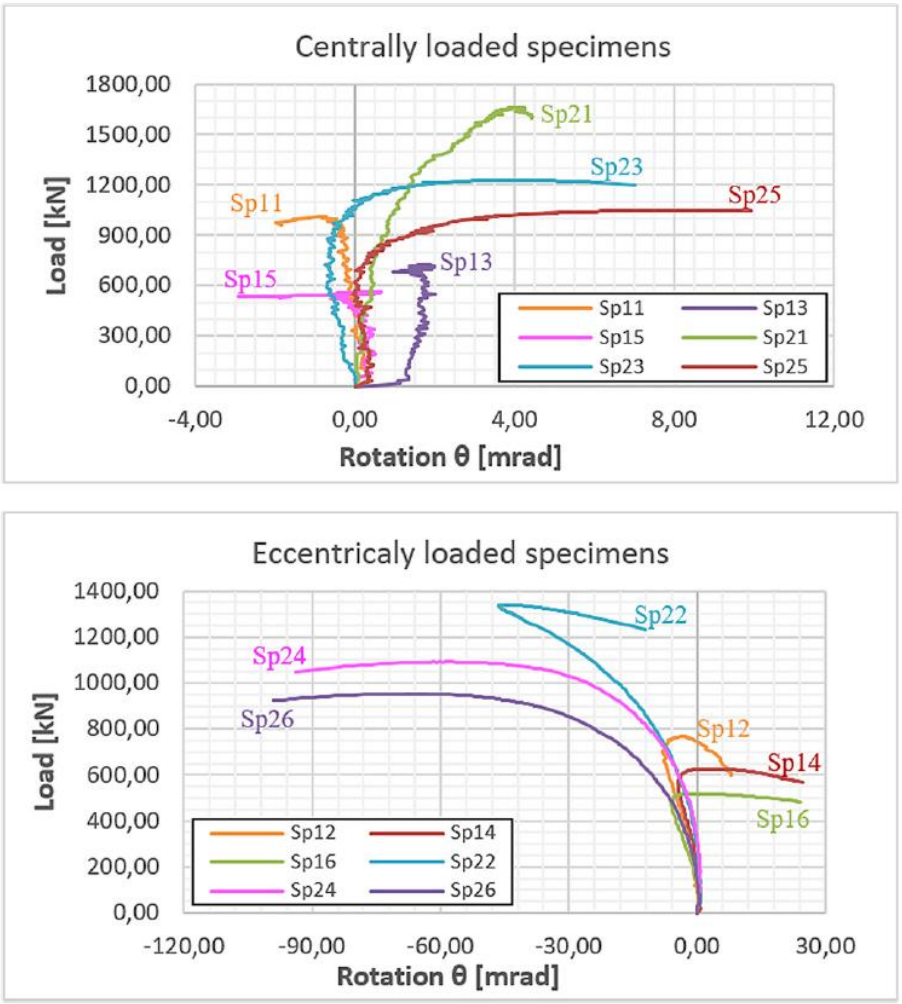

Fig. 14. Load-twist curves at mid-height cross-section for centrally loaded (up) and eccentrically loaded (down) specimens.

Published in : Thin-Walled Structures (2021), vol. 159, 107287
DOI: 10.1016/j.tws.2020.107287
Status : Postprint (Author's version)

(a) (b) (c)

Fig. 15. Final deformed shape of (a) Sp15 with a pure flexural buckling mode, (b) Sp26 with a flexural-torsional failure buckling mode and (c) Sp14 with a mixed mode between flexural and flexural torsional buckling.

Published in : Thin-Walled Structures (2021), vol. 159, 107287
DOI: 10.1016/j.tws.2020.107287
Status : Postprint (Author's version)

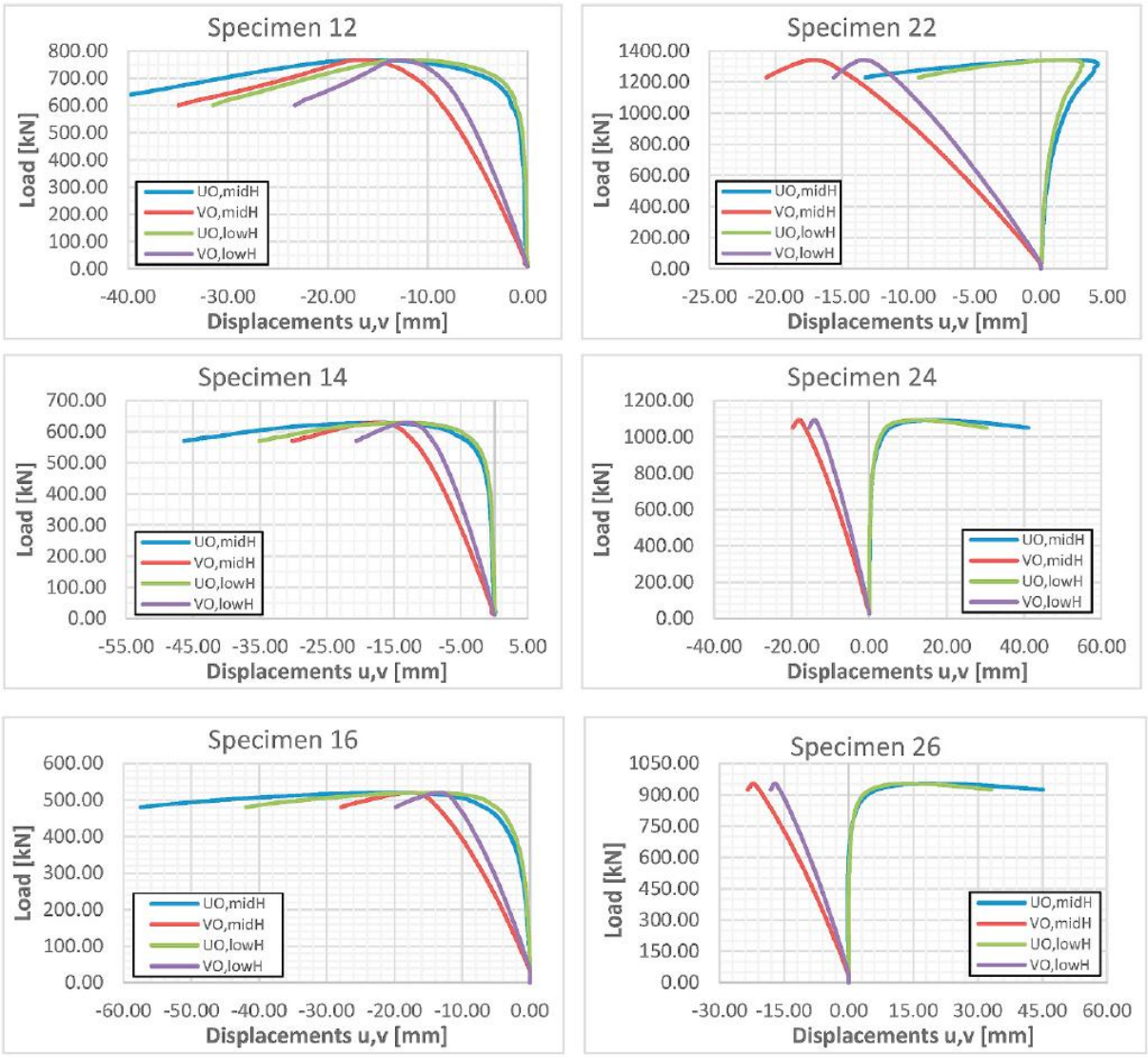

*U/VO,midH is the displacement of the corner point O of the mid – height cross-section along u/v principal axis

*U/VO,lowH is the displacement of the corner point O of the low – height cross-section along u/v principal axis

Fig. 16. Load-deflection curves for eccentrically loaded specimens.

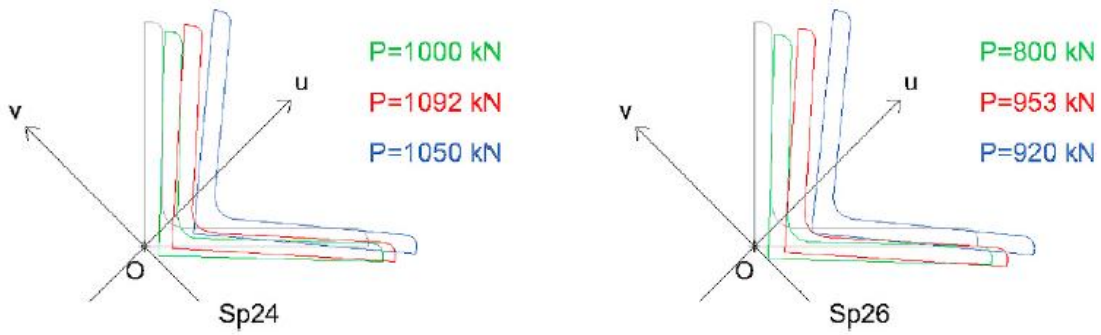

Fig. 17. Schematic movement of the mid-height cross-section along the loading for specimens Sp24 and Sp26.

Published in : Thin-Walled Structures (2021), vol. 159, 107287
DOI: 10.1016/j.tws.2020.107287
Status : Postprint (Author's version)

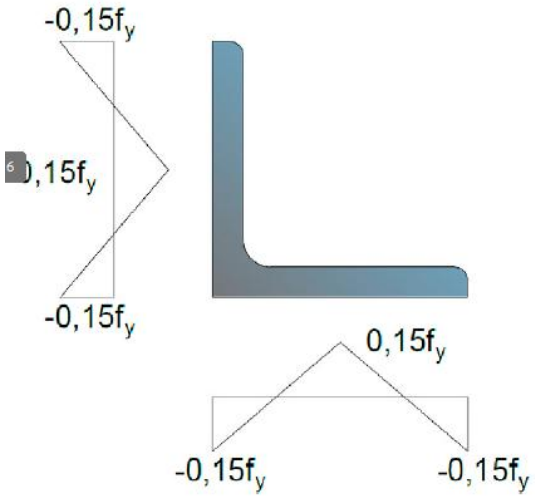

Fig. 18. Assumed distribution pattern of residual stresses based on Ref. [21,22].

Table 5
Deflections and twist at the mid-height cross-section at the failure load.

ID of Specimen	N_{exp} [kN]	u_O [mm]	v_O [mm]	θ [mrad]
Sp11	1010,6	8,88	-0,01	-0,82
Sp12	767,3	-15,28	-16,39	-3,94
Sp13	723,2	-28,22	0,53	1,71
Sp14	628,3	-16,35	-17,05	2,05
Sp15	563,9	-31,53	-0,95	0,39
Sp16	519,8	-17,78	-17,03	-1,81
Sp21	1661,5	10,89	1,52	3,96
Sp22	1341,4	2,48	-17,07	-44,92
Sp23	1228,0	20,49	1,53	3,51
Sp24	1092,3	16,87	-18,09	-59,51
Sp25	1048,1	-38,43	0,62	7,77
Sp26	953,6	16,31	-22,11	-62,95

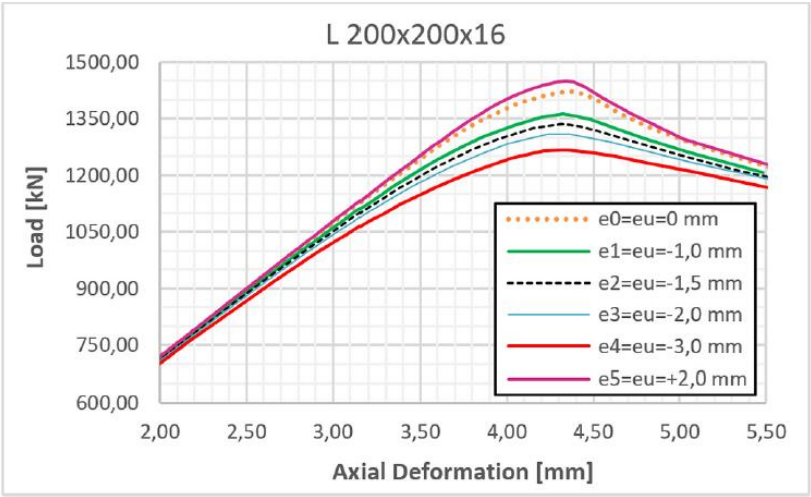

Fig. 19. Influence of eccentricity at the ultimate resistance of member (excerpt of the full graph).

Published in : Thin-Walled Structures (2021), vol. 159, 107287
DOI: 10.1016/j.tws.2020.107287
Status : Postprint (Author's version)

Fig. 20 and **Fig. 21** show the axial deformations (shortening) of the specimens versus the load for both experimental tests (solid lines) and numerical simulations (dotted lines). **Table 6** summarizes and compares the ultimate experimental and numerical resistances. One can see from the graphs and the table that there is a very good agreement between numerical simulations and experimental tests in terms of axial stiffness and load carrying capacity. The mean value of the ratio N_{exp}/N_{FEM} is equal to 0,98 with a COV of 1%.

Fig. 22 and **Fig. 23** show some characteristic load-deflections curves of the specimens for both experimental tests and numerical simulations.

The numerical results provide similar responses for most of the specimens without nominal loading eccentricity (same as Specimen Sp15 in **Fig. 22**), as well as a good correspondence with the tests. However, for two specimens (Sp21, Sp23), the numerical response appears to be more flexible than the test, at least in the first part of the test; but close to the failure, a rather good agreement with the experiment is contemplated.

Similar results, in terms of lateral flexibility of the columns, have been observed for eccentrically loaded specimens (see **Fig. 23**). This additional flexibility could be explained by the fact that the end plates at the extremities of the angle members have been modelled indirectly (additional length and restraints at the extremities of the member), as well as by the consideration of the unintentional eccentricities. The prevailing of weak axis buckling near the failure load has been observed also through the numerical simulations for the eccentrically loaded specimens.

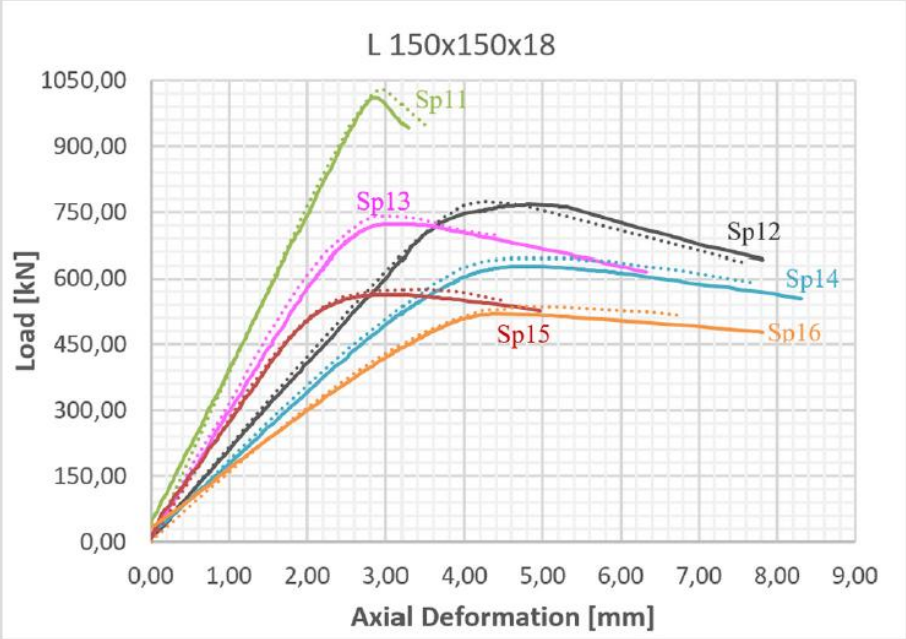

Fig. 20. Comparison between test and FEM results for Sp1#.

Published in : Thin-Walled Structures (2021), vol. 159, 107287
DOI: 10.1016/j.tws.2020.107287
Status : Postprint (Author's version)

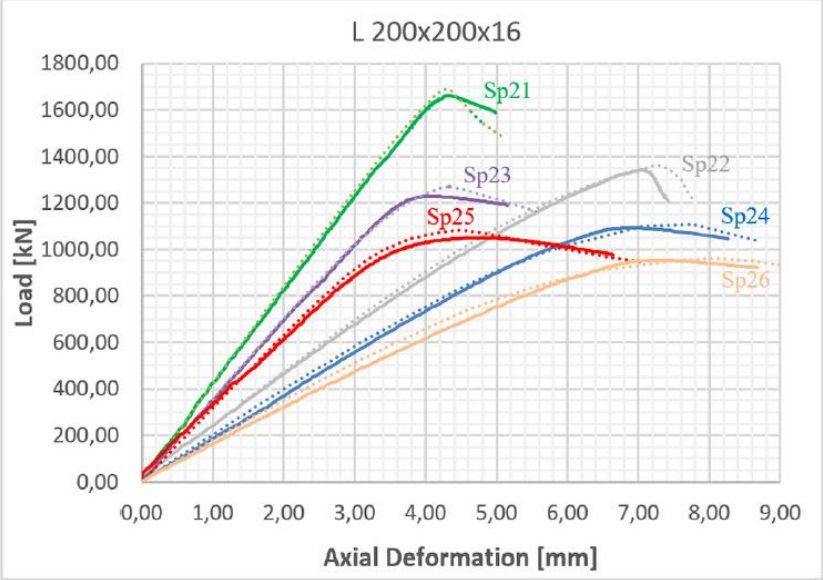

Fig. 21. Comparison between test and FEM results for Sp2#.

4.3. COMPARISON WITH THE PREDICTIONS OF EN 1993-1-1

In the following, the test results have been compared with the relevant Eurocode 3 predictions. Since many provisions have been changed during the development of the 2nd ongoing version of the Eurocodes, the analyses have been based on EN 1993-1-1: 2005, as well as the latest version of the Code available to the authors, namely prEN 1993-1- 1:2019 [23]. Hereafter, a unique reference to "EN 1993-1-1" means that there is no difference between the two versions.

According to EN 1993-1-1, the first profile (L 150 × 150 × 18) is classified as Class 1 and the second one (L 200 × 200 × 16) as Class 4. The procedure of EN 1993-1-5 [24] has been followed to evaluate the effective cross-section of the Class 4 profile, even if no plate buckling has been reported during the tests.

4.3.1. CENTRALLY LOADED SPECIMENS

According to EN 1993-1-1, the buckling resistance for centrally loaded angle members is calculated by the equation:

$$N_{EC3} = \chi \cdot (\rho \cdot A) \cdot f_v \qquad (7)$$

where:

χ is the buckling reduction factor which should be determined as a function of the relative slenderness $\overline{\lambda}$ of the compression member; A is the area of the cross-section;

ρ is the ratio $\rho = A_{eff}/A$, where the effective area of the cross-section is defined in Ref. [24];

f_y is the material yielding strength.

The non-dimensional slenderness $\overline{\lambda}$ is equal to:

Published in : Thin-Walled Structures (2021), vol. 159, 107287
DOI: 10.1016/j.tws.2020.107287
Status : Postprint (Author's version)

$$\bar{\lambda} = \sqrt{\frac{\rho \cdot A \cdot f_y}{N_{cr}}} = \sqrt{\frac{N_{pl}}{N_{cr}}} \quad (8)$$

Where N_{cr} is the elastic critical load for the relevant buckling mode (i.e. the minimum eigenvalue amongst all flexural and flexural-torsional buckling modes) obtained by an elastic instability analysis considering actual material (Young modulus), gross cross-section properties and buckling length, using FINELG software. For all centrally loaded specimens, the calculated eigenmode was a flexural buckling one. A pure torsional mode cannot be obtained for a centrally loaded angle column as explained in Ref. [19]. The actual yielding stress f_y (see **Table 4**) has been used in **eq. (7)** and **eq. (8)**.

The only difference of both aforementioned norms concerning the buckling resistance of centrally loaded members is in the selection of the buckling curves. EN 1993-1-1(2005) indicates curve b for all hot-rolled angle cross-sections independently of the buckling axis, while prEN 1993-1-1(2019) recommends curve b for steel grades S235 to S420 and curve a for S460 up to S700. **Table 7** includes the results of the calculations, with the assumption that specimens Sp11, Sp13 and Sp15 are S420 (based on the actual yield stress – buckling curve b) and Sp21, Sp23 and Sp25 are S460 (buckling curve a). In **Table 7** as in the rest of the paper, the subscript EC3 refers to EN 1993-1-1 (2005) and EC3' to prEN 1993-1-1 (2019).

Fig. 24 illustrates the experimental results (only for centrally loaded specimens) compared with those obtained through the recommendations of EN 1993-1-1; reference buckling curves a_0, a and b are reported too. The buckling reduction factor χ_{exp} of specimens has been evaluated by the equation:

$$\chi_{exp} = \frac{N_{exp}}{N_{pl}} \quad (9)$$

and the slenderness $\overline{\lambda_u}$ using **eq. (8)**. The results from the calculations presented in **Fig. 24** are shown in **Table 8**.

In EN 1993-1-1(2005), the buckling curve b has been selected for axially loaded equal angle columns (solid line in **Fig. 24**). It has been found that the experimental results are in line with this curve or above for specimens Sp1#, but are much higher for specimens Sp2#. In addition, it can be easily observed that the actual ultimate resistance of all centrally loaded columns is higher than the predictions of Eurocode; the later seems to provide safe evaluations, especially for specimens Sp2# where the detrimental effect of local buckling are possibly overestimated. Based on prEN 1993-1-1(2019), buckling curve b has been again selected for specimens Sp1# and the results are the same as before. However, when buckling curve a is used for Sp2#, the difference between the experimental and design resistance according to EC3 is smaller, as shown in **Table 8**.

Published in : Thin-Walled Structures (2021), vol. 159, 107287
DOI: 10.1016/j.tws.2020.107287
Status : Postprint (Author's version)

Table 6
Ultimate resistances obtained by experimental tests and numerical models.

ID of Specimen	Buckling length in GMNIA [mm]	Actual load eccentricitied [mm]	Additional assumed eccentricities in GMNIA [mm]	N_{exp} [kN]	N_{FEM} [kN]	$N_{exp}/N_{FEM}[-]$
Sp11	2607	0,00	$e_u = 1,50$	1010,6	1028,6	0,98
Sp12	2607	$e_v = 48,71$	$e_u = 0,50$	767,3	774,1	0,99
Sp13	3107	0,00	$e_u = -2,00$	723,2	739,3	0,98
Sp14	3107	$e_v = 48,72$	$e_u = -1,10$	628,3	645,9	0,97
Sp15	3607	0,00	$e_u = -2,00$	563,9	575,8	0,98
Sp16	3607	$e_v = 48,70$	$e_u = -1,00$	519,8	536,0	0,97
Sp21	3107	0,00	$e_u = -1,50$	1661,5	1690,6	0,98
Sp22	3107	$e_v = 66,60$	$e_u = -0,80$	1341,4	1361,0	0,99
Sp23	3607	0,00	$e_u = -2,00$	1228,0	1267,4	0,97
Sp24	3607	$e_v = 66,65$	$e_u = -0,50$	1092,3	1107,6	0,99
Sp25	4107	0,00	$e_u = -1,70$	1048,1	1082,2	0,97
Sp26	4107	$e_v = 66,63$	$e_u = 0,00$	953,6	959,1	0,99

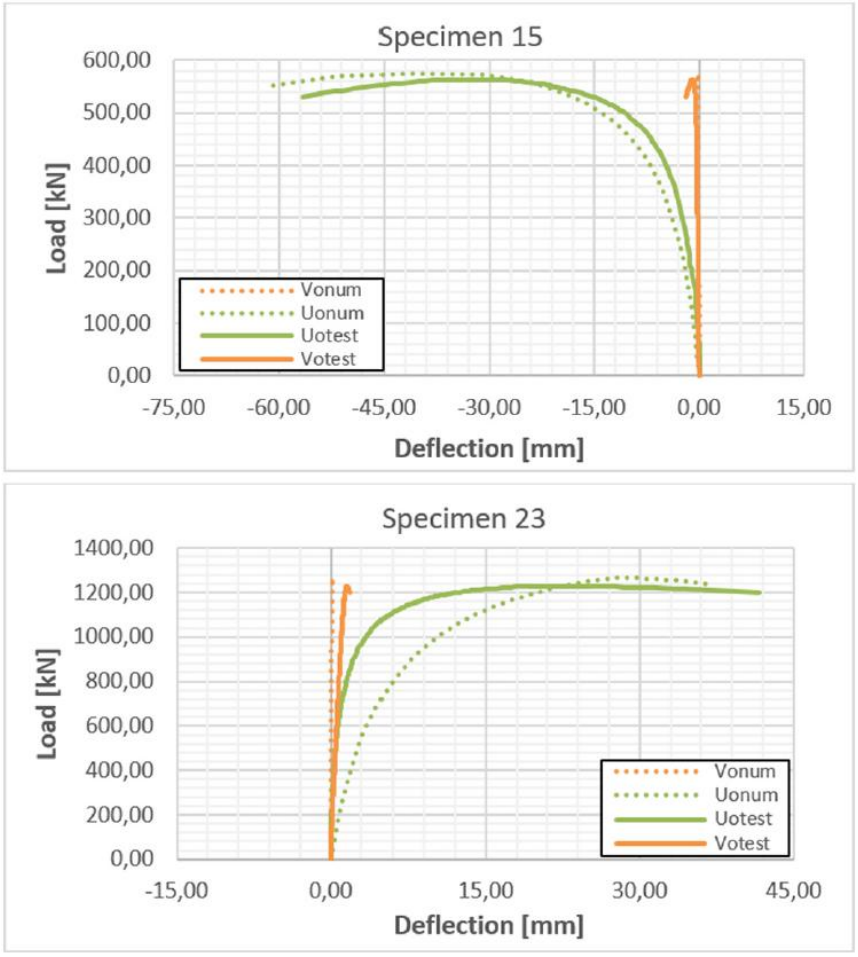

Fig. 22. Characteristic load-deflection curves at mid-height cross-section for centrally loaded specimens.

Published in : Thin-Walled Structures (2021), vol. 159, 107287
DOI: 10.1016/j.tws.2020.107287
Status : Postprint (Author's version)

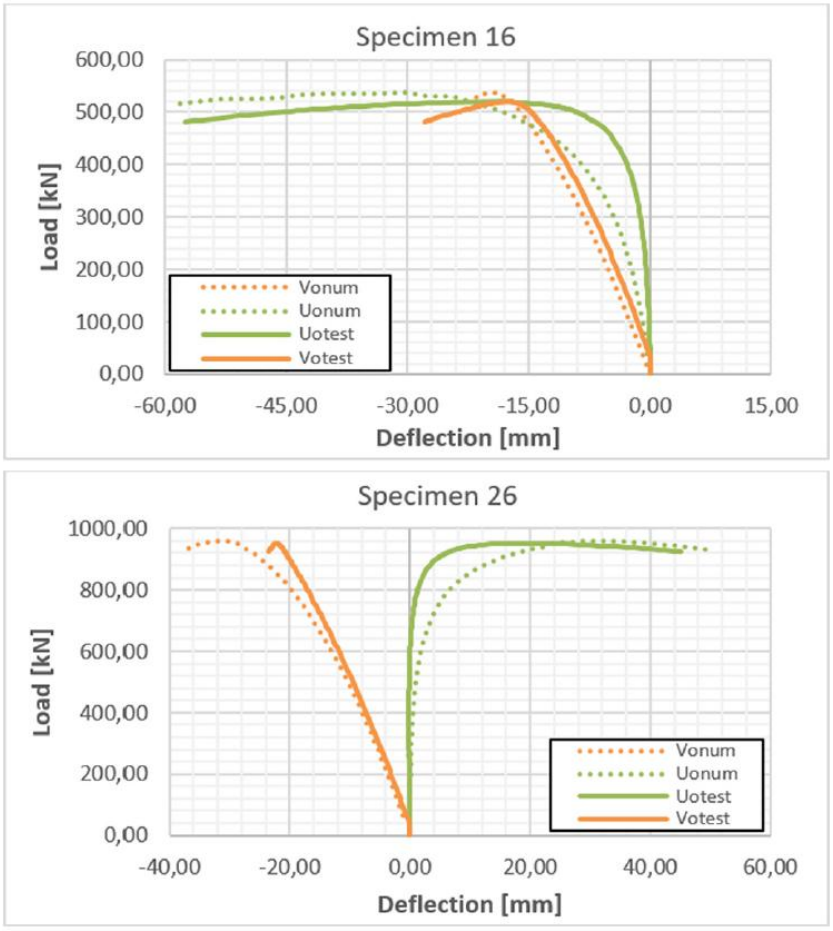

Fig. 23. Characteristic load-deflection curves at mid-height cross-section for eccentrically loaded specimens.

4.3.2. ECCENTRICALLY LOADED SPECIMENS

The general method of Eurocode 3 can be applied to evaluate the resistance of the eccentrically loaded angle members subjected to axial force and bending moments. In this case, the out-of-plane buckling resistance of the member is sufficient if the following equation satisfies:

$$\chi_{op} \cdot a_{ult,k} \geq 1,0 \qquad (10)$$

where: χ_{op} is the reduction factor corresponding to the non-dimensional slenderness $\overline{\lambda_{op}}$ and aimed at accounting for lateral and lateral torsional buckling, i.e. $\chi_{op} = \min\{\chi_b, \chi_{LT}\}$;

$a_{ult,k}$ is the minimum load amplifier of the design loads to reach the characteristic resistance of the most critical cross-section of the structural component considering its in plane behaviour without taking lateral or lateral torsional buckling into account however accounting for all effects due to in plane geometrical deformation and imperfections, global and local, where relevant. It can be derived from **eq. (11)**:

$$\frac{1}{\alpha_{ult,k}} = \frac{\sigma_{max}}{f_y} = \frac{\sigma_N}{f_y} + \frac{\sigma_{e_0}}{f_y} + \frac{\sigma_M}{f_y} \qquad (11)$$

In which:

Published in : Thin-Walled Structures (2021), vol. 159, 107287
DOI: 10.1016/j.tws.2020.107287
Status : Postprint (Author's version)

- the first term relates to the stress under pure compression;
- the second, to the second order maximum stress resulting from the amplification of the first order moment $N_{Ed}\cdot e_0$ (e_0 is the equivalent imperfection as defined in Eurocode 3), i.e. the moment $N_{Ed}\cdot e_0[1/(1- N_{Ed}/N_{cr,u})]$;
- the third one relates to the second order maximum stress resulting from the amplification of the first order moment $N_{Ed}\cdot e_v$ (e_v is the load eccentricity), which can be estimated as $N_{Ed}\cdot e_v[1/(1-N_{Ed}/N_{cr,u})]$.

The load eccentricity (e_v) resulted in strong axis bending, while geometrical equivalent imperfections (e_0) around both axes. However, the latter were smaller than the former, so that finally the effects of load eccentricity prevailed.

The global relative slenderness $\overline{\lambda_{op}}$ for the structural component should be determined from **eq. (12)**, in which the term $\alpha_{cr,op}$ is the minimum load amplifier for the in-plane design loads to reach the elastic critical load of the structural component associated to lateral or lateral torsional buckling without accounting for in-plane flexural buckling.

$$\overline{\lambda_{op}} = \sqrt{\frac{\alpha_{ult,k}}{\alpha_{cr,op}}} \qquad (12)$$

Regarding both versions of EN 1993-1-1, the difference is again in the selection of the buckling curves, but also here in the value of the equivalent imperfection e_0. The calculations according to EN 1993-1-1 (2005)-§6.3.4 and prEN 1993-1-1(2019)-§8.3.4 have been done and their results are reported in **Table 9** and **Table 10** respectively. Factors and parameters that are the same for both calculations are presented only in **Table 9**. Additionally, a recalculation has been done for each specimen, so as to evaluate the analytical load for which **eq. (10)** satisfies ($\chi_{op}\cdot\alpha_{ult,k}$ = 1,0). The obtained analytical estimations of the failure loads have then been compared to the experimental ones; the results are represent in **Table 11**.

Based on the results, one may conclude that the general method of Eurocode 3 is over-conservative even in its 2019 revised version.

Table 7
Calculation of member resistance according to EN 1993-1-1(2005)-§6.3.1 and prEN 1993-1-1(2019)-§8.3.1

ID of specimen	A [mm^2]	ρ [−]	N_{cr} [kN]	N_{pl} [kN]	$\bar{\lambda}$ [−]	χ_{EC3} [−]	N_{EC3} [kN]	$\chi_{EC3'}$ [−]	$N_{EC3'}$ [kN]
Sp11	5100,0	1,00	1233,73	2127,72	1313	0,4206	894,81	0,4206	894,81
Sp13	5101,1	1,00	894,30	2172,05	1558	0,3216	698,50	0,3216	698,50
Sp15	5106,5	1,00	663,55	2471,35	1810	0,2496	542,72	0,2496	542,72
Sp21	6180,2	0,845	2040,91	2567,47	1117	0,5251	1337,23	0,5844	1488,20
Sp23	6181,3	0,837	1515,05	2567,93	1290	0,4316	1088,60	0,4758	1200,16
Sp25	6180,1	0,845	1168,61	2567,43	1476	0,3513	894,11	0,3828	974,40

*EC3 = EN 1993-1-1 (2005), EC3' = prEN 1993-1-1 (2019).

Published in : Thin-Walled Structures (2021), vol. 159, 107287
DOI: 10.1016/j.tws.2020.107287
Status : Postprint (Author's version)

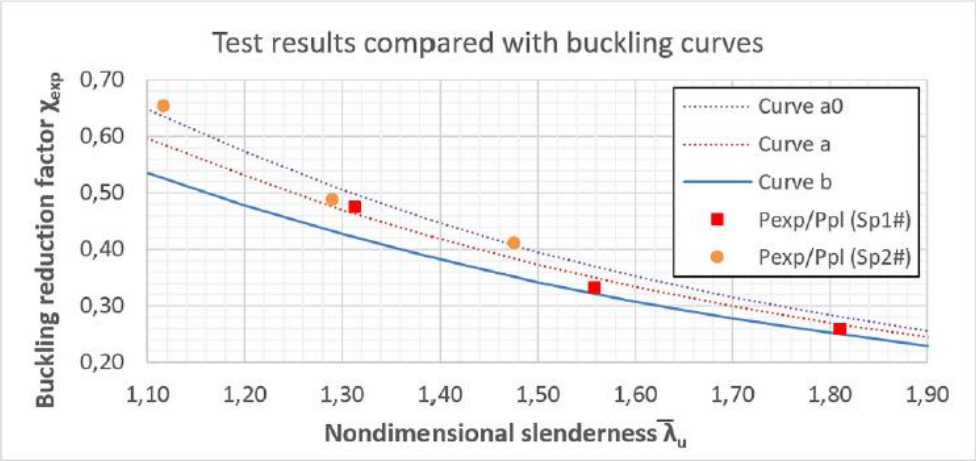

Fig. 24. Comparison of experimental results with buckling curves of EN 1993- 1-1.

Table 8
Comparison of experimental and normative reduction factors χ

ID of specimen	$\bar{\lambda}_u$ [−]	$\chi_{exp} = \frac{N_{exp}}{N_{pl}}$ [−]	χ_{exp}/χ_{EC3} [−]	$\chi_{exp}/\chi_{EC3'}$ [−]
Sp11	1313	0,4750	1,13	1,13
Sp13	1558	0,3330	1,04	1,04
Sp15	1810	0,2593	1,04	1,04
Sp21	1117	0,6472	1,24	1,12
Sp23	1290	0,4782	1,13	1,02
Sp25	1476	0,4082	1,17	1,08

*EC3 = EN 1993-1-1 (2005), EC3' = prEN 1993-1-1 (2019).

5. Conclusions

From the present study involving experimental, numerical and analytical aspects, the following conclusions may be drawn.

- The centrically loaded specimens with class 1 cross-section (Sp11, Sp13, Sp15) and the eccentrically loaded specimens with class 4 cross-section (Sp22, Sp24, Sp26) failed very clearly in a pure weak axis flexural buckling mode and correspondingly flexural torsional buckling mode.
- The centrically loaded specimens with class 4 cross-section (Sp21, Sp23, Sp25) and the eccentrically loaded specimens with class 1 cross-section (Sp12, Sp14, Sp16) failed mostly in a flexural torsional buckling mode, which was more pronounced in the former.
- Local buckling was not visibly observed in any specimen, although some of them were categorised as class 4 according to EN 1993-1-1.
- A very good agreement between the numerical GMNIA simulations and the experimental results in terms of axial stiffness and ultimate resistances has been achieved, through the consideration of an unintentional small eccentricity.

Published in : Thin-Walled Structures (2021), vol. 159, 107287
DOI: 10.1016/j.tws.2020.107287
Status : Postprint (Author's version)

- A small eccentricity of the position of the applying load can affect the ultimate resistance of the member in comparison with the perfect "no loading eccentricity" case. For the current study, an eccentricity equals to 1,5 mm may reduce the ultimate resistance by about 6%.
- The design resistance of the concentrically specimens based on EN 1993-1-1 (2005) is on the safe side, especially for the second profile for which the local buckling reduction effects seem to be overestimated by Eurocode. The results conform better with the application of the 2nd generation of the Eurocode 3, namely prEN 1993-1- 1:2019.
  The tests and the numerical simulations indicate, that it is more reasonable to calculate the member resistance of rolled angles by using the slenderness for flexural buckling only and not based on the "relevant buckling mode" which includes torsional effects, as EN 1993-1-1 prescribes.
- For eccentrically loaded columns, the general method recommended by Eurocode 3 appears as over-conservative.

It should be noted that the conclusions may are limited to the tested specimens, but a wider study is in progress to investigate the classification and design formulae, covering this time the whole domain of application, including different profiles, width-to-thickness ratios, steel grades and member lengths.

Table 9
Calculation of member resistance according to EN 1993-1-1(2005)-§6.3.4

ID of specimen	Sp12	Sp14	Sp16	Sp22	Sp24	Sp26
A [mm^2]	5133,30	5133,30	5148,30	6316,00	6290,70	6297,20
ρ [−]	1,00	1,00	1,00	0,845	0855	0,844
$N_{cr,u}$ [N]	4927795,5	3469382,9	2577221,6	8135740,3	5844997,9	4636928,4
e_0 [mm]	10,43	12,43	14,43	12,43	14,43	16,43
N_{Ed} [N]	767340,0	628270,0	519760,0	1341350,0	1092280,0	953620,0
σ_{max} [N/mm^2]	491,17	420,57	361,80	917,45	762,91	704,79
$\alpha_{ult,k}$ [−]	0,8669	1,0124	1,1769	0,5315	0,6195	0,6918
$\alpha_{cr,wab}$ [−]	1666	1,4331	1,2870	1,5601	1,3764	1,2507
χ_b [−] ($\alpha_{wab} = 0,34$)	0,7716	0,6991	0,6250	0,8452	0,7999	0,7584
$\alpha_{cr,LT}$ [−]	1,4483	1,3557	1,2372	1,1921	1,1370	1,0834
χ_{LT} [−] ($\alpha_{LT} = 0,76$)	0,5960	0,5413	0,4798	0,6644	0,6185	0,5803
$\chi_{op}\cdot\alpha_{ult,k}$ [−]	0,517	0548	0,565	0353	0,383	0401

Table 10
Calculation of member resistance according to prEN 1993-1-1(2019)-§8.3.4

ID of specimen	Sp12	Sp14	Sp16	Sp22	Sp24	Sp26
e_0 [mm]	10,85	12,93	15,01	8,54	9,77	11,29
σ_{max} [N/mm^2]	493,59	423,00	364,19	884,72	730,32	672,32
$\alpha_{ult,k}$ [−]	0,8627	1,0066	1,1692	0,5511	0,6468	0,7253
χ_b [−] ($\alpha_b = 0,34/0,21$ for Sp1#/Sp2#)	0,7726	0,7007	0,6270	0,8921	0,8545	0,8170
χ_{LT} [−] ($\alpha_{LT} = 0,76$)	0,5972	0,5428	0,4815	0,6563	0,6083	0,5686
$\chi_{op}\cdot\alpha_{ult,k}$ [−]	0,515	0546	0,563	0362	0,393	0412

Published in : Thin-Walled Structures (2021), vol. 159, 107287
DOI: 10.1016/j.tws.2020.107287
Status : Postprint (Author's version)

Table 11
Comparison of experimental and analytical loads evaluated with the general method.

ID of specimen	$N_{anal,EC3}$ [kN]	$N_{anal,EC3'}$ [kN]	$N_{exp}/N_{anal,EC3}$ [−]	$N_{exp}/N_{anal,EC3'}$ [−]
Sp12	410,0	408,6	1,87	1,88
Sp14	356,0	355,0	1,76	1,77
Sp16	303,3	302,3	1,71	1,72
Sp22	500,5	511,5	2,68	2,62
Sp24	442,5	453,2	2,47	2,41
Sp26	405,5	415,0	2,35	2,30

*EC3 = EN 1993-1-1 (2005), EC3' = prEN 1993-1-1 (2019).

CRediT author statement

Bezas Marios-Zois: Writing - original draft, Investigation, Software, Validation Demonceau Jean-François: Methodology, Investigation, Formal analysis Vayas Ioannis: Conceptualization, Supervision, Writing - review & editing Jaspart Jean-Pierre: Conceptualization, Supervision, Writing - review & editing

Declaration of competing interest

The authors declare that they have no known competing financial interests or personal relationships that could have appeared to influence the work reported in this paper.

Acknowledgments

The work presented here is carried in the framework of a European Research project entitled ANGELHY "Innovative solutions for design and strengthening of telecommunications and transmission lattice towers using large angles from high strength steel and hybrid techniques of angles with FRP strips", with a financial grant from the Research Fund for Coal and Steel (RFCS) of the European Community. Partners of the project were NTUA, ULiège, ArcelorMittal, CTICM, COSMOTE and SIKA France. The authors gratefully acknowledge this financial support.

Published in : Thin-Walled Structures (2021), vol. 159, 107287
DOI: 10.1016/j.tws.2020.107287
Status : Postprint (Author's version)

References

[1] EN 1993-3-1, Design of Steel Structures - Part 3-1: Towers, Musts and Chimneys. Tower and Musts, Brussels, Comité Européen de Normalisation (CEN), 2005.
[2] EN 1993-1-1, Design of Steel Structures - Part 1-1: General Rules and Rules for Buildings, Comité Européen de Normalisation (CEN), Brussels, 2005.
[3] EN 1993-1-8, Design of Steel Structures - Part 1-8: Design of Joints, Comité Européen de Normalisation (CEN), Brussels, 2005.
[4] EN 50341-1, Overhead Electrical Lines Exceeding AC 1 kV - Part 1, General requirements - Common specifications, 2012.
[5] Load and Resistance Factor Specifications for Single-Angle Members, AISC, 2000.
[6] H.Y. Ban, G. Shi, Y.J. Shi, Y.Q. Wang, Column buckling tests of 420MPa high strength steel single equal angles, Int. J. Struct. Stabil. Dynam. 13 (Issue 2) (2013), 1250069-1–1250069-23.
[7] A. Spiliopoulos, M.-E. Dasiou, P. Thanopoulos, I. Vayas, Experimental tests on members made from rolled angle sections, Steel Construction – Design and Research 11 (Issue 1) (2018) 84–93.
[8] M. Kettler, H. Unterweger, Laboratory tests on bolted steel angles in compression with varying end support conditions, Stahlbau 88 (H5) (2019) 447–459.
[9] M. Reininghaus, M. Skottke, Dimensioning of pressed angle steel with one screw joint based on the standards DIN 18800 vol2 and EC1993-3-1 (towers and masts), Stahlbau 74 H7 (2005) pp534–538, 40 tests.
[10] R. Haidar, Compressive Strength of Steel Single Angles Loaded through Two-Bolts in One Leg, MSc Thesis, University of Windsor, 1996.
[11] M. Shani, Compressive Strength of Eccentrically Loaded Steel Angles, MSc Thesis, University of Windsor, 1998.
[12] EN 1993-1-8, Design of Steel Structures - Part 1-8: Design of Joints, Brussels. Comité Européen de Normalisation (CEN), 2005.
[13] M.Z. Bezas, J.P. Jaspart, J.F. Demonceau, N. Labeye, Report about the Compression Tests on Large Angle Columns in High Strength Steel, Research Report-ANGELHY Project, University of Liège, 2020.
[14] EN 1090-2, Technical Requirements for the Execution of Steel Structures, Comité Européen de Normalisation (CEN), 2008.
[15] prEN 1993-1-14 (20XX): XXXX, Comité Européen de Normalisation (CEN), Brussels, 2018.
[16] EN ISO 6892 – 1, Metallic Materials – Tensile Testing – Part 1: Method of Test at Room Temperature, Brussels, Comité Européen de Normalisation (CEN), 2016.
[17] I.S.O.377 EN, Steel and Steel Products — Location and Preparation of Samples and Test Pieces for Mechanical Testing, Comité Européen de Normalisation (CEN), Brussels, 1997.
[18] FINELG, Non-linear Finite Element Analysis Program, User's Manual, Version 9.0, Greisch Ingeniere, 2003.
[19] V. de Ville de Goyet, L'analyse statique non linéaire par la méthode des éléments finis des structures spatiales formées de poutres à section non symétrique, PhD thesis, University of Liège, 1989.
[20] L. Zhang, J.P. Jaspart, Stability of Members in Compression Made of Large Hot- Rolled and Welded Angles, Research Report, University of Liège, 2013.
[21] P. Moze, L.G. Cajot, F. Sinur, K. Rejec, D. Beg, Residual stress distribution of large steel equal leg angles, Eng. Struct. 71 (2014) 35–47.
[22] A.A. de Menezes, S. da, P.C.G. Vellasco, L.R.O. de Lima, A.T. da Silva, Experimental and numerical investigation of austenitic stainless steel hot-rolled angles under compression, J. Constr. Steel Res. 152 (2019) 42–56.
[23] prEN 1993-1-1, Design of Steel Structures - Part 1-1: General Rules and Rules for Buildings, Comité Européen de Normalisation (CEN), Brussels, 2019.
[24] EN 1993-1-5, Design of Steel Structures - Part 1-5: Plate Structural Elements, Brussels, Comité 000, Europeen de Normalisation (CEN), 2006.